Amino Acids (2009) 37:725–732
DOI 10.1007/s00726-008-0201-z

ORIGINAL ARTICLE

Source of oseltamivir resistance in avian influenza H5N1 virus with the H274Y mutation

Maturos Malaisree · Thanyada Rungrotmongkol · Nadtanet Nunthaboot · Ornjira Aruksakunwong · Pathumwadee Intharathep · Panita Decha · Pornthep Sompornpisut · Supot Hannongbua

Received: 1 August 2008 / Accepted: 16 October 2008 / Published online: 12 November 2008

Abstract Molecular dynamics simulations were carried out for the mutant oseltamivir-NA complex, to provide detailed information on the oseltamivir-resistance resulting from the H274Y mutation in neuraminidase (NA) of avian influenza H5N1 viruses. In contrast with a previous proposal, the H274Y mutation does not prevent E276 and R224 from forming the hydrophobic pocket for the oseltamivir bulky group. Instead, reduction of the hydrophobicity and size of pocket in the area around an ethyl moiety at this bulky group were found to be the source of the oseltamivir-resistance. These changes were primarily due to the dramatic rotation of the hydrophilic $-COO^-$ group of E276 toward the ethyl moiety. In addition, hydrogen-bonding interactions with N1 residues at the $-NH_3^+$ and -NHAc groups of oseltamivir were replaced by a water molecule. The calculated binding affinity of oseltamivir to NA was significantly reduced from -14.6 kcal mol^{-1} in the wild-type to -9.9 kcal mol^{-1} in the mutant-type.

Keywords Oseltamivir resistance · H274Y mutation · Neuraminidase · H5N1

Introduction

The outbreak of avian influenza A (H5N1) viruses has raised global concern for animal and human health. Recently, isolates of the virus with amino acid changes in neuraminidase (NA) that likely confer the reduction in susceptibility to oseltamivir have been reported (Reece 2007; McKimm-Breschkin et al. 2007; Ferraris and Lina 2008). In order to have a better chance of overcoming these and predicting probable new resistance problems, an understanding of the mechanism of oseltamivir resistance at the molecular level is required.

The influenza viral NA is a receptor-destroying enzyme that cleaves a terminal sialic acid and releases viral progeny from infected cells, and has been separated into two groups by genetic and structural relationships: group-1 NA includes N1, N4, N5 and N8, whereas group-2 NA includes N2, N3, N6, N7, and N9. Based on the crystal structures, group-1 NA differs from group-2 NA by having a large cavity close to the active site on the 150-loop, at residues 147-152 (Russell et al. 2006). However, the active site in all subtypes is conserved. The catalytic sites (R118, D151, D152, R224, E276, R292, R371 and Y406) were found to interact with the sialic acid while the framework sites (E119, R156, W178, S179, D198, I222, E227, H274, E277, N294, and E425) (in N2 numbering) were supposed to stabilize the active site structure (Colman et al. 1983).

M. Malaisree and T. Rungrotmongkol have contributed equally to this work.

Electronic supplementary material The online version of this article (doi:10.1007/s00726-008-0201-z) contains supplementary material, which is available to authorized users.

M. Malaisree · T. Rungrotmongkol · P. Intharathep · P. Decha · P. Sompornpisut · S. Hannongbua (✉)
Department of Chemistry, Faculty of Science, Chulalongkorn University, Patumwan, Bangkok 10330, Thailand
e-mail: supot.h@chula.ac.th

N. Nunthaboot
Department of Chemistry, Faculty of Science, Mahasarakham University, Mahasarakham 44150, Thailand

O. Aruksakunwong
Department of Chemistry, Faculty of Science, Rangsit University, Pathumtani 12000, Thailand

NA has been targeted for improved anti-influenza drugs. The approved NA inhibitors were designed on a basis of the transition state analog of sialic acid complexed with group-2 NA (De Clercq 2006). Two marketable NA inhibitors, zanamivir and oseltamivir, are available for treatment of influenza virus infections (Moscona 2005b). To date, high resistance and mutations against oseltamivir have been widely reported, not only in vitro and in vivo but also in clinical treatment. Mutations in group-1 NA (N1) were detected at H274Y and N294S (Ives et al. 2002; de Jong et al. 2005; Le et al. 2005; Wang et al. 2002; Kiso et al. 2004; Mishin et al. 2005; Yen et al. 2007) and in group-2 NA (N2 and N9) at E119V, I222V and R292K (Baz et al. 2006; Carr et al. 2002). In H5N1 subtypes of the virus, the H274Y mutation in the NA active site leads to a high-level resistance to oseltamivir, typically with a 300- to 1,700-fold reduction in susceptibility (Ives et al. 2002; de Jong et al. 2005; Le et al. 2005; Wang et al. 2002; Kiso et al. 2004; Mishin et al. 2005; Yen et al. 2007). The proposed mechanism of oseltamivir resistance caused by the H274Y mutation is that the hydrophobic pocket around the bulky oseltamivir group, which is generally created by the rotation of the E276 side chain to bind with the R224 side chain, cannot be formed (McKimm-Breschkin et al. 2001; Moscona 2005a; von Itzstein 2007). However, detailed information on the results of such proposed changes has not been identified in molecular level.

To provide detailed information on the primary source of oseltamivir-resistance due to the H274Y mutation, molecular dynamics (MD) simulations have been carried out for the mutant type of NA complexed with oseltamivir. The results were analyzed in terms of conformational changes, intra- and intermolecular hydrogen bonds, ligand solvation and binding free energy of the complex, focused on the catalytic pocket of NA. These structural and molecular properties were compared and discussed extensively with our previous study on the wild-type N1 complexed with oseltamivir (Malaisree et al. 2008).

Materials and methods

Molecular dynamics simulations

The crystal structure of the NA subtype N1 complexed with oseltamivir (2HU4.pdb) (Russell et al. 2006) was used as the initial structure. To prepare the H274Y mutant for inhibitor binding (OTV-MT), the N1 residue 274 was changed from histidine to tyrosine using the LEaP module of the AMBER 7 software package (Case et al. 2002). All missing hydrogen atoms of the protein and inhibitor were added with standard bond lengths and angles. The ionization states of amino acids with electrically charged side chains were assigned using the PROPKA program (Li et al. 2005). The system was solvated with a TIP3P water box (Jorgensen et al. 1983) and neutralized by the counterions. The total number of atoms in the periodic box of 78 Å × 80 Å × 81 Å was 41,302.

All calculations were performed using AMBER 7 (Case et al. 2002). The Cornell force field (Cornell et al. 1995) was applied for the amino acids while the partial atomic charges and force-field parameter of the inhibitor were taken from our previous calculations (Malaisree et al. 2008). A time step of 2 fs was used with a cut-off radius of 12 Å for the non-bonded interactions. The particle mesh Ewald method was used for calculating the long-range electrostatic interactions (York et al. 1993). The periodic boundary MD simulations were performed with the NPT ensemble. A Berendsen coupling time of 0.2 ps was used to maintain the temperature and pressure of the system (Berendsen et al. 1984). The SHAKE algorithm (Ryckaert et al. 1997) was employed to constrain all bonds involving hydrogen.

To remove bad contacts, locations of hydrogen atoms and the added water molecules were initially optimized, and then energy minimization of the entire system was carried out. Afterward, the MD simulations were performed over three periods: a thermalization phase from 0 to 298 K over 60 ps, an equilibration phase at 300 K for 1.5 ns, and the final production period for 1.5 ns. Only the snapshots taken from the production phase were used for analysis. The convergence of energies, temperature, pressure, and global root mean square deviation (RMSD) were used for verification of the system stability.

Binding free energy calculations

To estimate the binding affinity between protein (NA) and ligand (oseltamivir), the free energy was calculated based on the Molecular Mechanics/Poisson-Boltzmann Surface Area (MM/PBSA) methodology (Srinivasan et al. 1998; Wang et al. 2001; Gilson et al. 1988), and implemented in AMBER 7. One hundred MD snapshots were extracted (at every 75 ps) from the production phase and were used as a structural ensemble to evaluate the MM/PBSA binding free energy. After all the water molecules and counterions were striped, the binding free energy of the protein–ligand complex (ΔG_{bind}) was computed by

$$\Delta G_{\text{bind}} = \Delta G_{\text{complex}} - \left[\Delta G_{\text{protein}} + \Delta G_{\text{ligand}}\right] \quad (1)$$

where $\Delta G_{\text{complex}}$, $\Delta G_{\text{protein}}$, and ΔG_{ligand} refer to the absolute free energy of the complex, protein, and ligand, respectively. Typically, the total free energy of a given conformational state i contains the enthalpy and entropy contributions and is expressed by

$$\Delta G_i = \Delta H_i - T\Delta S_i \quad (2)$$

where ΔH of a system is composed of the enthalpy changes in the gas phase upon complex formation (ΔE_{MM}) and the solvated free energy contribution (ΔG_{sol}) and $-T\Delta S$ refers to the entropy contribution to the binding. Therefore, Eq. 2 can be approximated as

$$\Delta G_i = \Delta E_{(MM)i} + \Delta G_{(sol)i} - T\Delta S_i \quad (3)$$

$\Delta E_{(MM)i}$ is further divided into van der Waals (ΔE_{vdW}) and electrostatic (ΔE_{ele}) interaction energies between the ligand and its receptor (Eq. 4). These interaction energies were calculated using the SANDER module in AMBER 7.

$$\Delta E_{MM} = \Delta E_{vdW} + \Delta E_{ele} \quad (4)$$

$\Delta G_{(sol)i}$ is composed of electrostatic $\left(\Delta G_{sol}^{ele}\right)$ and non-polar $\left(\Delta G_{sol}^{nonpolar}\right)$ contributions (Eq. 5).

$$\Delta G_{sol} = \Delta G_{sol}^{ele} + \Delta G_{sol}^{nonpolar}. \quad (5)$$

The Delphi4 program suite (Rocchia et al. 2001) was used to evaluate the electrostatic free energy of solvation. A grid spacing of 0.33 Å with the boundary condition of Debye-Hückel potentials was applied. Atomic charges were taken from the Cornell force field (Cornell et al. 1995). The dielectric values applied for water and protein were set to 80 and 1, respectively. The non-polar contribution to the solvation free energy is calculated according to the linear function of the solvent accessible surface area (SASA) (Eq. 6).

$$\Delta G_{sol}^{nonpolar} = \gamma SASA + b \quad (6)$$

where $\gamma = 0.00542$ kcal mol^{-1}Å^{-2}, and $b = 0.92$ kcal mol^{-1}.

In this study, the same set of coordinates for complex, protein, and ligand were used, and the entropy contribution was ignored as reported and justified in previous works (Prompers and Brüschweiler 2002; Saarela et al. 2002; Zhou et al. 2005; Ferrari et al. 2007).

Results and discussion

To evaluate the stability of the simulated systems, RMSDs of OTV-WT and OTV-MT complexes (all atoms) obtained during the 3-ns MD simulations relative to the initial structure were calculated and plotted in Fig. S1 (see supplementary materials). As can be seen from the RMSD plots, the two systems were found to reach equilibrium at 1.5 ns and, therefore, the MD trajectories extracted from the 1.5–3.0 ns simulations were used for the following analysis.

Conformational changes in the neighborhood of H274Y

In order to determine the effect of the H274Y mutation on the interactions between oseltamivir and the N1 active site, changes of the molecular conformations within the neighborhood of H274Y were monitored. Interpretations were focused on oseltamivir's 1-ethylproxy (–OCHEt$_2$), and the Y274, E276 and R224 side chains. The results are shown in Fig. 1b in terms of the torsional angles, *Tor-H274Y, Tor-E276, Tor-R224, Tor-X, Tor-Y, and Tor-Z*, defined by sets of four atoms (arrows in Fig. 1a). Here, the corresponding data from our previous oseltamivir-wild type (OTV-WT) simulations (Malaisree et al. 2008) are also given for comparison.

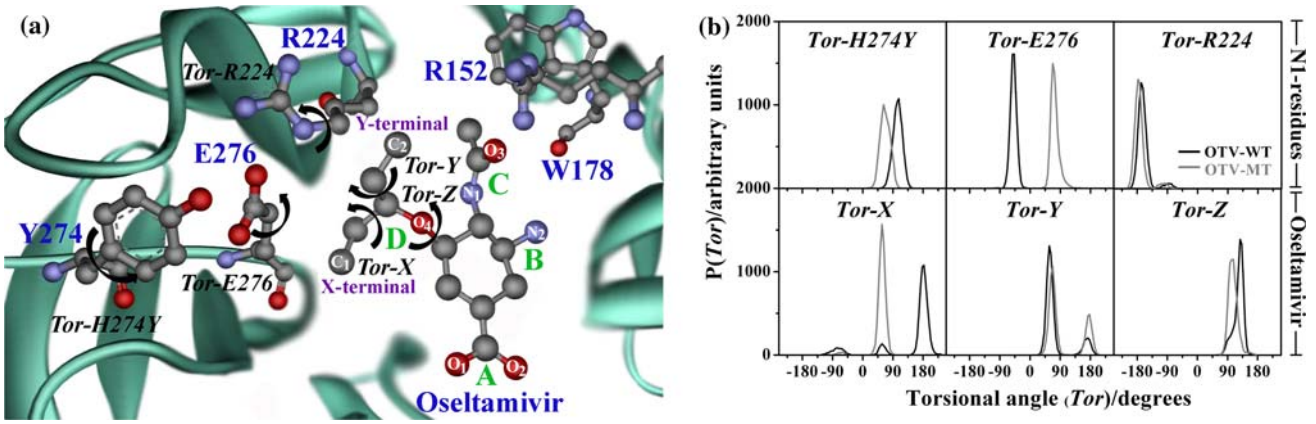

Fig. 1 **a** Model structure of the oseltamivir bound to the N1-H274Y mutation where R224, Y274 and E276 were shown in the ball and stick model, while locations of R152 and W178 were also given. The torsional angles of the side chains of residues H274Y, E276 and R224 were defined by *Tor-H274Y*, *Tor-E276* and *Tor-R224*, respectively, while those of the hydrophobic side chain of oseltamivir were described by *Tor-X*, *Tor-Y* and *Tor-Z*. **b** Plot of torsional angle distribution (*black* for wild type and *gray* for mutant type), sampling after equilibration at 1.5 ns

Considering the torsional angle of the side chain of residue 274 before and after mutation (Fig. 1b), *Tor-H274Y* of the histidine's immidazole ring in the OTV-WT complex exhibits a sharp peak at 107.5° (black line in Fig. 1b), which was altered to 62.5° for the *Tor-H274Y* of the tyrosine's phenyl ring in OTV-MT (gray line in Fig. 1b). This rotation and an apparent size increase of the side chain in changing from H274 to Y274 is supposed to lead to a rearrangement of the neighboring residues, R224 and E276 (Fig. 1a). Note that the formation of the hydrophobic pocket for the oseltamivir's bulky $-OCHEt_2$ side chain in the NA is determined by these two residues (McKimm-Breschkin et al. 2001; Moscona 2005a; von Itzstein 2007).

The meaningful changes after the H274Y mutation were found to control the new conformation of the E276's carboxylate group, where *Tor-E276* was noticeably shifted by 115° from −47.5° to 67.5° (Fig. 1b). This is due to the bulky side chain of Y274, where the molecular refractivity (parameter of bulkiness) of 31.83 for tyrosine is significantly larger than that of 23.79 for histidine (Sak et al. 1999). Changes of the E276 conformations were found to strongly influence the rotation and flexibility of the $-OCHEt_2$ group of oseltamivir. This fact is indicated by the appearance of a single sharp and narrow peak in *Tor-X* of the $-OCHEt_2$ side chain at the X-terminal in the OTV-MT complex at 57.5° (gray line in Fig. 1b). This is different from what is found for OTV-WT. The flexibility and rotation of this terminal is shown by the three peaks at −77.5°, 57.5°, and 182.5° (black line in Fig. 1b). A dramatic change in the preferential conformation of the X-terminal by 125° (from 182.5° for OTV-WT to 57.5° for OTV-MT) is clearly due to the rotation of *Tor-E276* (by 115° as described above). This means that the rotation brings the hydrophilic $-COO^-$ group of the E276 side chain to approach the X-terminal (see Fig. 1a) of the $-OCHEt_2$ group of oseltamivir and leads consequently to the reduction of the hydrophobic pocket of the N1 mutant (see Fig. S2 in supplementary materials). In other words, rotation of the $-CH_2CH_3$ moiety at the $-OCHEt_2$ group of oseltamivir was found to be induced by the reduction of the hydrophobicity of the catalytic pocket of N1. To clarify this point, structural alignment of the MD snapshots of both OTV–WT and OTV–MT complexes sampling every 0.5 ns after equilibration, was plotted in Fig. 2c. It can be seen that the E276 side chain was noticeably shifted toward the bulky moiety of oseltamivir while displacement of oseltamivir was also slightly exhibited. Consequently, this fact was found to induce some changes of the positions of two binding residues, R152 and W178, leading to the loss of their hydrogen bonds with oseltamivir (details in section of "loss of inhibitor-enzyme hydrogen bond").

Interestingly, the aforementioned remarkable changes do not cause significant changes to the $-OCHEt_2$ moiety at

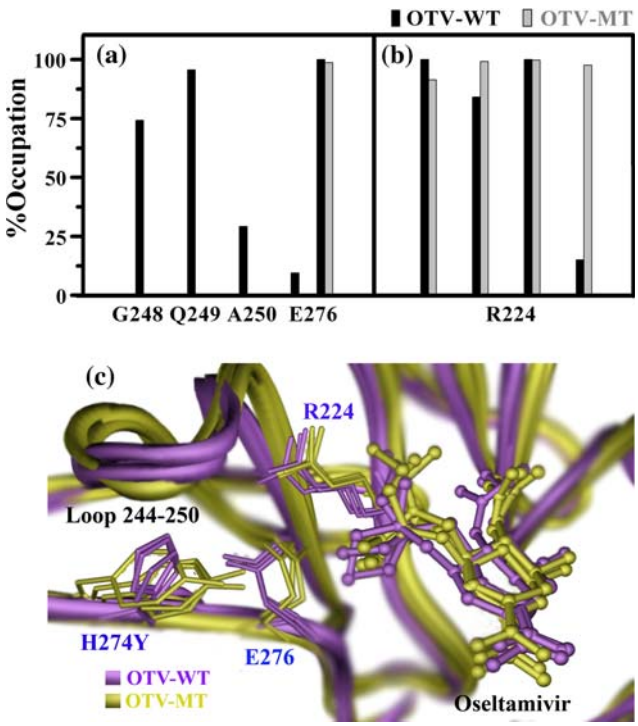

Fig. 2 Percentage occupation of hydrogen bonding of **a** the mutated residue 274 (H274Y) to its surrounding residues, and **b** between the carboxylate group of E276 and the guanidinium group of R224. **c** Structural alignment between the three MD snapshots of OTV–WT and OTV–MT sampling every 0.5 ns after equilibration phase. Close-up of oseltamivir, the two important residues R224 and E276, and the loop 244–250 located in the neighborhood of the mutated residue 274 are all shown

the Y-terminal and its contacted residue R224, suggesting that the conformation of this region is considerably conserved. In the results; *Tor-Y* and *Tor-R224,* which determine the rotations of the Y-terminal and the R224 side chain, respectively, for both OTV–WT and OTV–MT complexes were found at almost the same angles (Fig. 1a , b). In addition, a slight shift of the maximum of *Tor-Z* by 20° from 127.5° (for OTV–WT) to 107.5° (for OTV–MT) indicates a strong influence of the H274Y mutation, which can establish a rotation around the principal axis of the $-OCHEt_2$ group of oseltamivir.

Loss of intramolecular hydrogen bonds of the enzyme

To understand the effects of the H274Y mutation on the intramolecular interactions, percentage and number of hydrogen bonds between H274Y and its neighboring residues and between the two charged residues (E276 and R224) were determined, based on the following criteria: (1) the distance between proton donor (D) and acceptor (A) atoms was less than or equal to 3.5 Å and (2) the D-H….A angle was greater than or equal to 120°. The results were evaluated and given in Fig. 2 whereas details of hydrogen

bond type were shown in Table S1 in supplementary materials.

It is shown from the plots that the immidazole ring of H274 strongly interacts with the four residues G248, Q249, A250, and E276 through a hydrogen-bonding framework (black columns in Fig. 2a) in which this ring acted as the center of interactions. This is in contrast with what is found for OTV–MT, in which only one hydrogen bond with E276 was retained. Rotation of the *Tor-H274Y* by 62.5° in changing from the histidine's immidazole ring (OTV–WT: black line in Fig. 1b) to the tyrosine's phenyl ring (OTV–MT: gray line in Fig. 1b), as discussed above, was found to be the source for the loss of these hydrogen bonds. In addition, the results show that the loop containing residues 244–250 is considerably conserved (see Fig. 2c). Loss of the hydrogen bond framework in the region close to the bulky group of oseltamivir is likely to reduce the stability of the hydrophobic pocket and subsequently to lower the capacity of the oseltamivir binding to the N1 active site.

Surprisingly, four hydrogen bonds formed between E276 and R224 were observed for both OTV–WT and OTV–MT complexes (Fig. 2b), suggesting that the H274Y mutation does not reduce the attractive interaction between these two residues. This finding contradicts the previous hypothesis (McKimm-Breschkin et al. 2001; Moscona 2005a; von Itzstein 2007) which stated that the H274Y mutation inhibits the formation of the hydrophobic pocket around the bulky side chain of oseltamivir, i.e., hydrogen bonding between E276 and R224 cannot be formed in the H274Y complex. From our results, the H274Y mutation does not prevent the E276 and R224 from forming a pocket. As discussed above, reduction of the hydrophobicity of the catalytic pocket of N1 in the area around the X-terminal of the $–OCHEt_2$ moiety of oseltamivir is the primary source of the oseltamivir resistance.

Loss of inhibitor-enzyme hydrogen bond

Hydrogen bonding analysis was extended to determine the particular interactions between the inhibitor and its binding pocket residues, using the same criteria as mentioned above. From the histograms shown in Fig. 3a, numbers of hydrogen bonds are highly detected in the wild- and mutant-types, formed by R292, R371, Y347, E119, D151, W178, R152, and E277. Loss of inhibitor-enzyme hydrogen bonds, due to the H274Y mutation, takes place at W178 and R152 residues.

The results in Fig. 3 lead to a clear conclusion that the interaction with W178 and the one hydrogen bond with R152 (see Fig. 1a for their locations) were lost in the OTV–MT complex (see gray lines in Fig. 3a). This observation can be understood by the distribution plots of the related distances shown in Fig. 3b. With the distances of $\sim$3.0 Å (maxima of the first two black-line peaks in Fig. 3b), the nitrogen atoms of R152's guanidinium group in OTV-WT can form two strong hydrogen bonds with the carbonyl oxygen (O_3) of oseltamivir's –NHAc group (side C in Fig. 1a). This is different for the orientation of R152 in the OTV–MT complex, where the guanidinium group was flipped; one of the two nitrogen atoms was turned to be located $\sim$5.0 Å from the O_3-oxygen (see gray line in Fig. 3b) and, therefore, only one hydrogen bond remained. For the W178 residue, the loss of the hydrogen bond in OTV–MT is a consequence in the increase in the distance between the ammonium nitrogen (N_2) of oseltamivir and the backbone oxygen (O) of W178, from 3.7 Å in OTV–WT to 5.3 Å in OTV–MT. The question arose whether loss of the hydrogen bonds between oseltamivir and these two residues, R152 and W178, is due to the displacement of the oseltamivir. It can be clearly seen from Fig. 2c that oseltamivir in the mutant system does not move toward its $–OCHEt_2$ groups (side D in Fig. 1a).

Oseltamivir's solvation

The ligand solvation was monitored in terms of atom-atom radial distribution functions [RDFs, $g_{xy}(r)$—the probability of finding a particle of type y within a sphere radius r around the particle of type x]. The results as well as the running coordination numbers integrated up to the first minimum (marked by an arrow) of the corresponding RDF are summarized in Fig. 4. No change was found in terms of

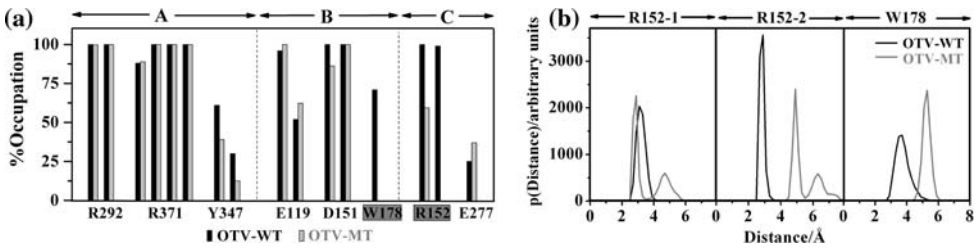

Fig. 3 **a** Percent occupation pattern of hydrogen bonds between residues in the binding pocket (labeled on the *x*-axis) and side chains A, B and C (defined in Fig. 1a) of the inhibitors for the two simulated systems, OTV–WT and OTV–MT. **b** The probability distributions of distance between specific atoms (see text for details) of the inhibitors and NA residues, R152 and W178, located in the active site of the oseltamivir

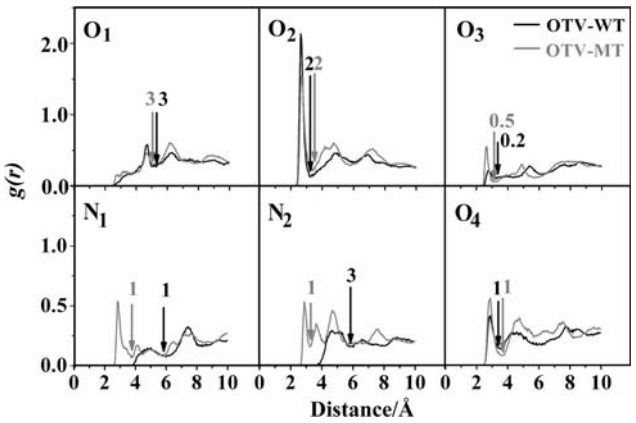

Fig. 4 Radial distribution functions, *g(r)*, centered on oseltamivir atoms, to water oxygen atoms of the OTV–WT and OTV–MT complexes. The corresponding running coordination numbers integrated up to their first minima (marked by *arrows*) are also given

both number and distribution of water molecules around the O_1- and O_2-oxygens on the carboxylate group (side A) and the O_4-oxygen on the bulky group (side D) of oseltamivir (atomic labels shown in Fig. 1a). Interest is focused on the N_1, N_2, and O_3 atoms on the $-NH_3^+$ (side B) and –NHAc (side C) groups of oseltamivir where solvation in the wild-type and mutant systems is considerably different. The three RDFs of OTV–MT show sharp first peaks centered at ~3.0 Å, with the corresponding coordination numbers of 1, 1, and 0.5 water molecules for the N_1, N_2, and O_3 atoms, respectively. Based on detailed analysis of the simulated trajectories, the three coordination numbers are found to result from one water molecule located in the vicinity of the $-NH_3^+$ and –NHAc side chains of oseltamivir. The situation is different for the OTV–WT complex, where water was found at distances longer than 4.0 Å from the two nitrogen atoms while the coordination number of 0.2 was observed for O_3. The simulation results lead us to conclude that these three atoms in OTV–MT were increasingly solvated. This can be a clear reason why sides B and C of oseltamivir lose their interactions with the R152 and W178 residues of the N1 enzyme (Fig. 3a).

Binding affinity of oseltamivir

The MM/PBSA-based binding free energies for the OTV–WT and OTV–MT complexes were calculated and separated into electrostatic (ΔE_{ele}), van der Waals, (ΔE_{vdw}), non-polar solvation $\left(\Delta G_{sol}^{nonpolar}\right)$ and electrostatic solvation $\left(\Delta G_{sol}^{ele}\right)$ components. The results are summarized in Table 1. As expected, the electrostatic energy, part of the ΔE_{MM}, makes a major contribution to the oseltamivir-enzyme binding. The H274Y mutation leads to a decrease in the $\Delta G_{binding}$ from -14.6 ± 4.3 kcal mol^{-1} to -9.9 ± 6.4 kcal mol^{-1}. The major contribution to the weaker binding affinity in the MT complex comes from the electrostatic solvation free energy term, 214.3 ± 10.3 kcal mol^{-1} compared with 206.0 ± 8.8 kcal mol^{-1} for OTV–WT. This is in agreement with the solvation data where more water molecules were found in the vicinity of oseltamivir in OTV–MT than that in OTV–WT. The observed trends, as well as the absolute values of the predicted binding free energies, are consistent with experimental studies (Yen et al. 2007) indicating the lower inhibitory potency of OTV to MT NA compared with WT NA.

Table 1 Calculated binding free energy and its components (kcal mol^{-1}) for the calculated OTV–WT and OTV–MT complexes

	OTV–WT	OTV–MT
ΔE_{ele}	-191.9 ± 10.5	-195.7 ± 11.2
ΔE_{vdw}	-28.8 ± 3.6	-28.5 ± 3.4
ΔE_{MM}	-220.6 ± 9.7	-224.2 ± 9.8
$\Delta G_{sol}^{nonpolar}$	-3.5 ± 0.1	-3.2 ± 0.4
ΔG_{sol}^{ele}	209.5 ± 8.8	217.5 ± 10.3
ΔG_{sol}	206.0 ± 8.7	214.3 ± 10.3
$\Delta G_{sol}^{ele} + \Delta E_{ele}$	17.6 ± 5.3	21.8 ± 7.5
$\Delta G_{binding}$	-14.6 ± 4.3	-9.9 ± 6.4
$\Delta G_{experiment}^{a}$	-13.0 ± 0.2	-8.6 ± 0.2

[a] $\Delta G_{experiment}$ was calculated from the IC_{50} (Yen et al. 2007) using the following relations

$\Delta G_{binding} = RT \ln K_{dissociation}$

$= RT \ln (IC_{50} + 0.5\ C_{enzyme})$

$\sim RT \ln IC_{50}$

Where R is the ideal gas constant, T is temperature in K, C_{enzyme} is the concentration of enzyme, which is a very small number after equilibration and can be omitted in most cases (Rizzo et al. 2002; Wang et al. 2001)

Conclusions

We have studied and compared the molecular and structural properties of the oseltamivir binding to both wild- and mutant types of avian influenza (H5N1) NA using the molecular dynamics simulation approach. The extensive analysis of OTV–MT and OTV–WT complexes was carried out with the simulated data obtained from the present study and previously calculated simulations (Malaisree et al. 2008), respectively. The results provide detailed information on the oseltamivir-resistance caused by the H274Y mutation at the molecular level. Within the N1 active site of OTV-MT, bulky side chain of the Y274 phenol ring drives the E276 carboxylate group to rotate away in a direction toward an ethyl moiety of oseltamivir's bulky group, resulting in a rather small hydrophobic pocket that is unable to accommodate this bulky group. This is

found to be the primary source of the oseltamivir-resistance associated with the H274Y mutation, which is in contrast with the proposed mechanism of oseltamivir-resistance to this particular mutation in H5N1 NA (McKimm-Breschkin et al. 2001; Moscona 2005a; von Itzstein 2007). The E276 side chain rotation confers the reduction of hydrophobicity at the bulky group. In addition, the $-NH_3^+$ and –NHAc groups of oseltamivir lose their hydrogen bonding interactions with the N1 residues, which was compensated by greater accessibility to water molecule at these two regions. This basic knowledge will be useful for the development and refinement of new antiviral inhibitors for a high potency against both wild-type and drug-resistant strains of neuraminidase N1.

Acknowledgments This work was supported by the Thailand Research Fund and the Royal Golden Jubilee Ph.D. Program (3.C.CU/48/F.1). T. R. thanks the Commission on Higher Education for the Post-Doctoral Program. The authors thank the Computational Chemistry Unit Cell, Chulalongkorn University and National Center for Genetic Engineering and Biotechnology (BIOTEC) for computing facilities. The National Nanotechnology Center (NANOTEC) supplied Discovery Studio for molecular graphics.

References

Baz M, Abed Y, McDonald J, Boivin G (2006) Characterization of multidrug resistant influenza A/H3N2 viruses shed during 1 year by an immunocompromised child. Clin Infect Dis 43:1555–1561. doi:10.1086/508777

Berendsen HJC, Postma JPM, van Gunsteren WF, DiNola A, Haak JR (1984) Molecular dynamics with coupling to an external bath. J Chem Phys 81:3684–3690. doi:10.1063/1.448118

Carr J, Ives J, Kelly J, Lambkin R, Oxford J, Mendel D, Tai L, Roberts N (2002) Influenza virus carrying neuraminidase with reduced sensitivity to oseltamivir carboxylate has altered properties in vitro and is compromised for infectivity and replicative ability in vivo. Antiviral Res 54:79–88. doi:10.1016/S0166-3542(01)00215-7

Case DA, Pearlman DA, Caldwell JW, Cheatham TEIII, Wang J, Ross WS, Simmerling CL, Darden TA, Merz KM, Stanton RV, Cheng AL, Vincent JJ, Crowley M, Tsui V, Gohlke H, Radmer RJ, Duan Y, Pitera J, Massova I, Seibel GL, Singh UC, Wiener PK, Kollman PA (2002) AMBER 7. University of California, San Francisco

Colman PM, Varghese JN, Laver WG (1983) Structure of the catalytic and antigenic sites in influenza virus neuraminidase. Nature 303:41–44. doi:10.1038/303041a0

Cornell WD, Cieplak P, Bayly CI, Gould IR, Merz KM, Ferguson DM, Spellmeyer DC, Fox T, Caldwell JW, Kollman PA (1995) A second generation force-field for the simulation of proteins, nucleic-acids, and organic-molecules. J Am Chem Soc 117:5179–5197. doi:10.1021/ja00124a002

De Clercq E (2006) Antiviral agents active against influenza A virus. Nat Rev Drug Discov 5:1015–1025. doi:10.1038/nrd2175

de Jong MD, Tran TT, Truong HK, Vo MH, Smith GJ, Nguyen VC, Bach VC, Phan TQ, Do QH, Guan Y, Peiris JS, Tran TH, Farrar J (2005) Oseltamivir resistance during treatment of influenza A (H5N1) infection. N Engl J Med 353:2667–2672. doi:10.1056/NEJMoa054512

Ferrari AM, Degliesposti G, Sgobba M, Rastelli G (2007) Validation of an automated procedure for the prediction of relative free energies of binding on a set of aldose reductase inhibitors. Bioorg Med Chem 15:7865–7877. doi:10.1016/j.bmc.2007.08.019

Ferraris O, Lina B (2008) Mutations of neuraminidase implicated in neuraminidase inhibitors resistance. J Clin Virol 41:13–19. doi:10.1016/j.jcv.2007.10.020

Gilson MK, Sharp KA, Honig BH (1988) Calculating the Electrostatic Potential of Molecules in Solution - Method and Error Assessment. J Comput Chem 9:327–335. doi:10.1002/jcc.540090407

von Itzstein M (2007) The war against influenza: discovery and development of sialidase inhibitors. Nat Rev Drug Discov 6:967–974. doi:10.1038/nrd2400

Ives JA, Carr JA, Mendel DB, Tai CY, Lambkin R, Kelly L, Oxford JS, Hayden FG, Roberts NA (2002) The H274Y mutation in the influenza A/H1N1 neuraminidase active site following oseltamivir phosphate treatment leave virus severely compromised both in vitro and in vivo. Antiviral Res 55:307–317. doi:10.1016/S0166-3542(02)00053-0

Jorgensen WL, Chandrasekhar J, Madura JD, Impey RW, Klein ML (1983) Comparison of simple potential functions for simulating liquid water. J Chem Phys 79:926–935. doi:10.1063/1.445869

Kiso M, Mitamura K, Sakai-Tagawa Y, Shiraishi K, Kawakami C, Kimura K, Hayden FG, Sugaya N, Kawaoka Y (2004) Resistant influenza A viruses in children treated with oseltamivir: descriptive study. Lancet 364:759–765. doi:10.1016/S0140-6736(04)16934-1

Le QM, Kiso M, Someya K, Sakai YT, Nguyen TH, Nguyen KH, Pham ND, Ngyen HH, Yamada S, Muramoto Y, Horimoto T, Takada A, Goto H, Suzuki T, Suzuki Y, Kawaoka Y (2005) Avian flu: isolation of drug-resistant H5N1 virus. Nature 437:1108. doi:10.1038/4371108a

Li H, Robertson AD, Jensen JH (2005) Very fast empirical prediction and interpretation of protein pKa values. Proteins 61:704–721. doi:10.1002/prot.20660

Malaisree M, Rungrotmongkol T, Decha P, Intharathep P, Aruksakunwong O, Hannongbua S (2008) Understanding of known drug-target interactions in the catalytic pocket of neuraminidase subtype N1. Proteins 71:1908–1918. doi:10.1002/prot.21897

McKimm-Breschkin JL, Sahasrabudhe A, Blick T, McDonald M (2001) Mechanisms of resistance of influenza virus to neuraminidase inhibitors. Int Congr Ser 1219:855–861. doi:10.1016/S0531-5131(01)00364-8

McKimm-Breschkin JL, Selleck PW, Usman TB, Johnson MA (2007) Reduced sensitivity of influenza A (H5N1) to oseltamivir. Emerg Infect Dis 13:1354–1357

Mishin VP, Hayden FG, Gubareva LV (2005) Susceptibilities of antiviral-resistant influenza viruses to novel neuraminidase inhibitors. Antimicrob Agents Chemother 49:4515–4520. doi:10.1128/AAC.49.11.4515-4520.2005

Moscona A (2005a) Oseltamivir resistance-disabling our influenza defenses. N Engl J Med 353:2633–2636. doi:10.1056/NEJMp058291

Moscona A (2005b) Neuraminidase inhibitors for influenza. N Engl J Med 353:1363–1373. doi:10.1056/NEJMra050740

Prompers JJ, Brüschweiler R (2002) Dynamic and structural analysis of isotropically distributed molecular ensembles. Proteins 46:177–189. doi:10.1002/prot.10025

Reece PA (2007) Neuraminidase inhibitor resistance in influenza viruses. J Med Virol 79:1577–1586. doi:10.1002/jmv.20951

Rizzo RC, Udier-Blagović M, Wang DP, Watkins EK, Kroeger Smith MB, Smith RH Jr, Tirado-Rives J, Jorgensen WL (2002) Prediction of activity for nonnucleoside inhibitors with HIV-1

reverse transcriptase based on Monte Carlo simulations. J Med Chem 45:2970–2987. doi:10.1021/jm010580q

Rocchia W, Alexov E, Honig B (2001) Extending the applicability of the nonlinear Poisson-Boltzmann equation: multiple dielectric constants and multivalent ions. J Phys Chem B 105:6507–6514. doi:10.1021/jp010454y

Russell RJ, Haire LF, Stevens DJ, Collins PJ, Lin YP, Blackburn GM, Hay AJ, Gamblin SJ, Skehel JJ (2006) The structure of H5N1 avian influenza neuraminidase suggests new opportunities for drug design. Nature 443:45–49. doi:10.1038/nature05114

Ryckaert JP, Ciccotti G, Berendsen HJ (1997) Numerical integration of the Cartesian equations of motion of a system with constraints: molecular dynamics of n-alkanes. J Comput Phys 23:327–341. doi:10.1016/0021-9991(77)90098-5

Saarela JT, Tuppurainen K, Peräkylä M, Santa H, Laatikainen R (2002) Correlative motions and memory effects in molecular dynamics simulations of molecules: Principal components and rescaled range analysis suggest that the motions of native BPTI are more correlated than those of its mutants. Biophys Chem 95:49–57. doi:10.1016/S0301-4622(01)00250-2

Sak K, Karelson M, Järv J (1999) Modeling of the amino acid side chain effects on peptide conformation. Bioorg Chem 27:434–442. doi:10.1006/bioo.1999.1150

Srinivasan J, Cheatham TEIII, Cieplak P, Kollman PA, Case DA (1998) Continuum solvent studies of the stability of DNA, RNA, and phosphoramidate-DNA helices. J Am Chem Soc 120:9401–9409. doi:10.1021/ja981844+

Wang J, Morin P, Wang W, Kollman PA (2001) Use of MM-PBSA in reproducing the binding free energies to HIV-1 RT of TIBO derivatives and predicting the binding mode to HIV-1 RT of Efavirenz by docking and MM-PBSA. J Am Chem Soc 123:5221–5230. doi:10.1021/ja003834q

Wang MZ, Tai CY, Mendel DB (2002) Mechanism by which mutations at His274 alter sensitivity of influenza A virus N1 neuraminidase to oseltamivir carboxylate and zanamivir. Antimicrob Agents Chemother 46:3809–3816. doi:10.1128/AAC.46.12.3809-3816.2002

Yen HL, Ilyushina NA, Salomon R, Hoffmann E, Webster RG, Govorkova EA (2007) Neuraminidase inhibitor-resistant recombinant A/Vietnam/1203/04 (H5N1) influenza viruses retain their replication efficiency and pathogenicity in vitro and in vivo. J Virol 81:12418–12426. doi:10.1128/JVI.01067-07

York DM, Darden TA, Pedersen LG (1993) The effect of long-range electrostatic interactions in simulations of macromolecular crystals: a comparison of the Ewald and truncated list methods. J Chem Phys 99:8345–8348. doi:10.1063/1.465608

Zhou Z, Madrid M, Evanseck JD, Madura JD (2005) Effect of a bound non-nucleoside RT inhibitor on the dynamics of wild-type and mutant HIV-1 reverse transcriptase. J Am Chem Soc 127:17253–17260. doi:10.1021/ja053973d